Chapter 2. Methods

Resumen capítulo 2:

Métodos

En este capítulo se describen todas las técnicas empleadas para medir los distintos parámetros oculares en los modelos animales implementados en esta tesis. En particular, se diseñó y construyó un sensor de frente de onda Hartmann-Shack para medir las aberraciones oculares de pollos y ratones adaptados a las características propias de cada modelo. Además un biómetro de ultrasonidos fue adaptado para las medidas de longitud axial en ojos de pollo y se construyó un queratómetro (en colaboración con Alberto de Castro) adaptándolo a las pequeñas dimensiones del ojo del pollo para una medida correcta de la curvatura corneal. El error refractivo fue medido mediante retinoscopía de mano o bien por aberrometría en algunos estudios de pollos o ratones donde la retinoscopía no era posible.

In this chapter we describe all the techniques to measure different ocular parameters in animal model eyes implemented in this thesis. In particular we designed and built a Hartmann-Shack wavefront sensor to measure ocular aberrations in chicks and mice, adapted to the particular features of these models. We also adapted an ultrasound biometer to measure axial length in the chick eye, and built (in collaboration with Alberto de Castro) a keratometer adapted to small eye dimensions to measure corneal curvature in the chick eye. Refractive error was obtained by streak retinoscopy or from aberrometry in some chick and mice studies were retinoscopy was not possible.

2.1. Measurement of ocular aberrations

We measured ocular monochromatic aberrations in animal models using a custom-developed Hartmann-Shack wavefront sensor, built specifically in this thesis for this application.

In the Hartmann-Shack technique a light point source is projected on the retina, and the light reflected is focused by a microlens array on a CCD camera (see Figure 1.8 on the introduction). Deviations of each retinal spot with respect to the ideal location are obtained in order to reconstruct the wave aberration in the pupil plane. In this section we present the design, set up, calibration and computer routines for automatic control and data processing developed in this thesis. The system was built with the following specifications: 1) It should be adapted to the animal eye dimensions (chick and mouse); 2) It should be compact and easily portable (for example, to an animal facility) and installable on any computer.

2.1.1. Hartmann Shack set- up

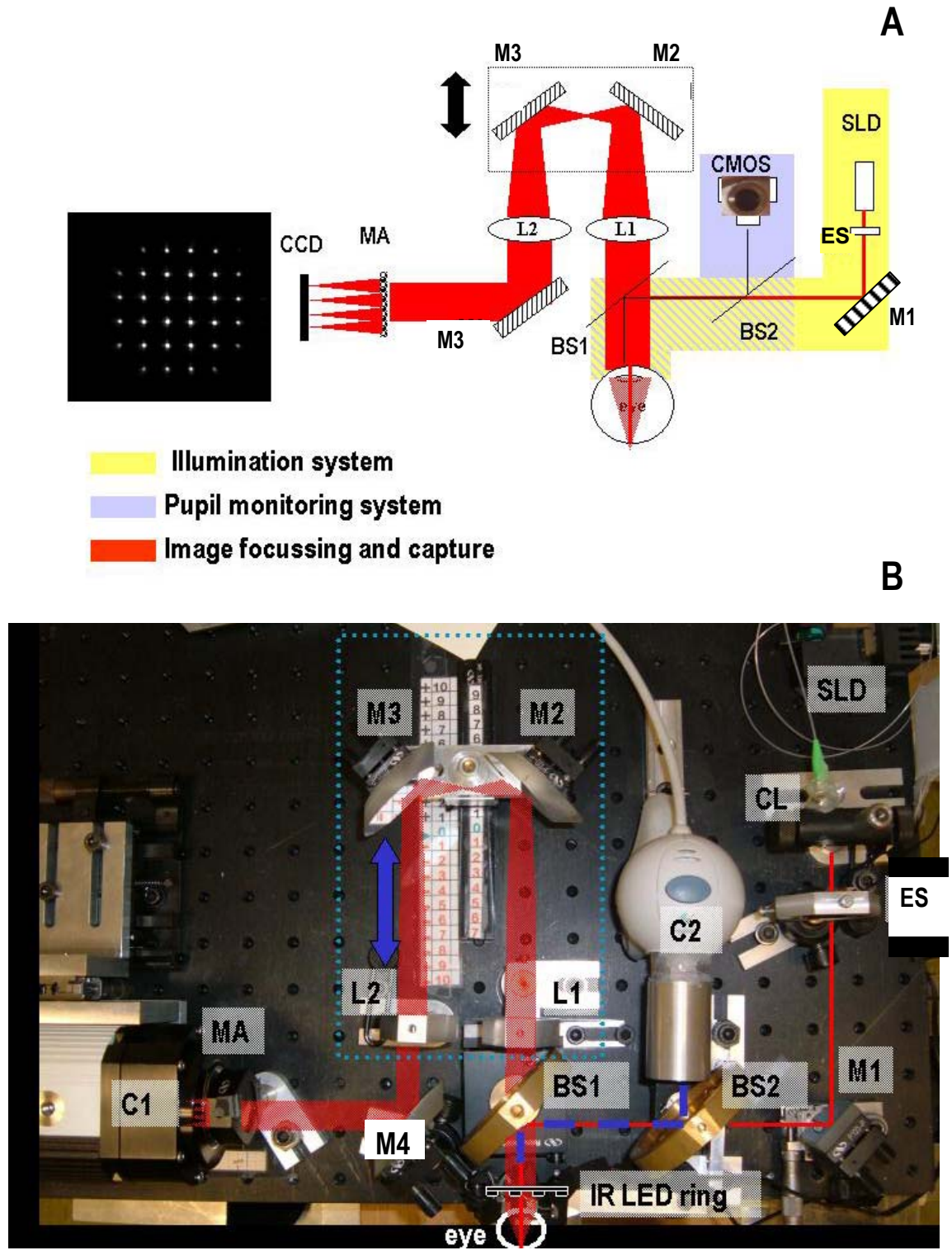

Figure 2.1 Schematic diagram (A) and photograph (B) of the custom-built Hartmann-Shack system.

We developed a Hartmann-Shack aberrometer with three channels: Illumination channel, detection channel, and pupil monitoring channel. The system was mounted on an aluminium optic table (AOSA, Madrid, Spain) and the physical dimensions of the optical sep up were 35 x 50 mm. The optical table was mounted on a x-y-z stage, so that the entire platform (rather than the animal) was moved for pupil centration (x-y) and pupil focus (z). Figure 2.1 A & B shows a schematic diagram and photograph of the system.

2.1.1.1. Illumination channel

The illumination channel projects a light spot onto the retina. The light source consists of a Superluminiscent Diode (SLD) (Superlum Diodes Ltd. Moscow, Russia) with an emission wavelength of 676 ± 14.6 nm. A module driving set for current and temperature control for the SLD allowed light intensity adjustment. The SLD was coupled to fibre optic attached to a collimator lens (CL) (Thorlabs, Munich, Germany) (see Figure 2.2). At the exit of the lens, the light beam has a 0.22º half angle of divergence and 6.2 mm diameter. The beam is blocked by an electronic shutter (ES) (Densitron technologies, London, United Kingdom) to control light exposure. The device consisted on a single blade shutter driven by a solenoid plunger. When power was applied the shutter was closed and it opened when the power was turned off. The shutter open and close time was less than 16 ms. The shutter was controlled from the computer by data acquisition modules (ADAM).

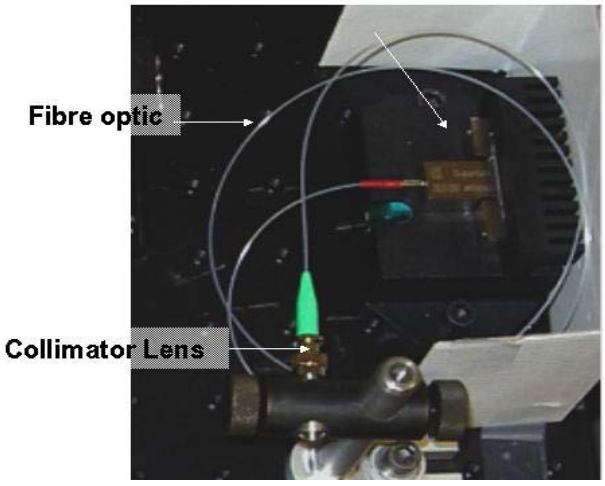

Figure 2.2 Super Luminiscent Diode (SLD)

When the shutter was opened, the light beam from the SLD was directed into the eye by reflections on a square silver mirror (M1) (Newport

Corporation, Irving, California, USA) and a plate beam splitter (BS1) (Melles Griot, Rochester, New York, USA). Exposure levels and times were below maximum values for human eyes, following ANSI safety standards.

2.1.1.2. Detection channel

The detection channel consisted of: 1) a 25-mm circular lenslet array (MA) (Adaptive Optics Associates, Inc, Cambridge MA, USA) with a square pattern of microlenses (65 columns x 65 rows) of 400 microns aperture and 24-mm focal length on a epoxy substrate. The filling material was an anti-reflection coating that provides less than 0.5% of reflection. 2) A cooled high resolution (1280 x 1024 pixels) 12 bit CCD camera (C1) (Retiga 1300. Qimaging, Burnaby, Canada), with high signal to noise ratio (60 dB)). The camera was provided with a firewire interface, plug and play capabilities and high speed data transfer rate. 3). A focusing block (FB) that consisted of a Badal system with two elliptical mirrors (M2 & M3) of 33.02 and 46.70 mm

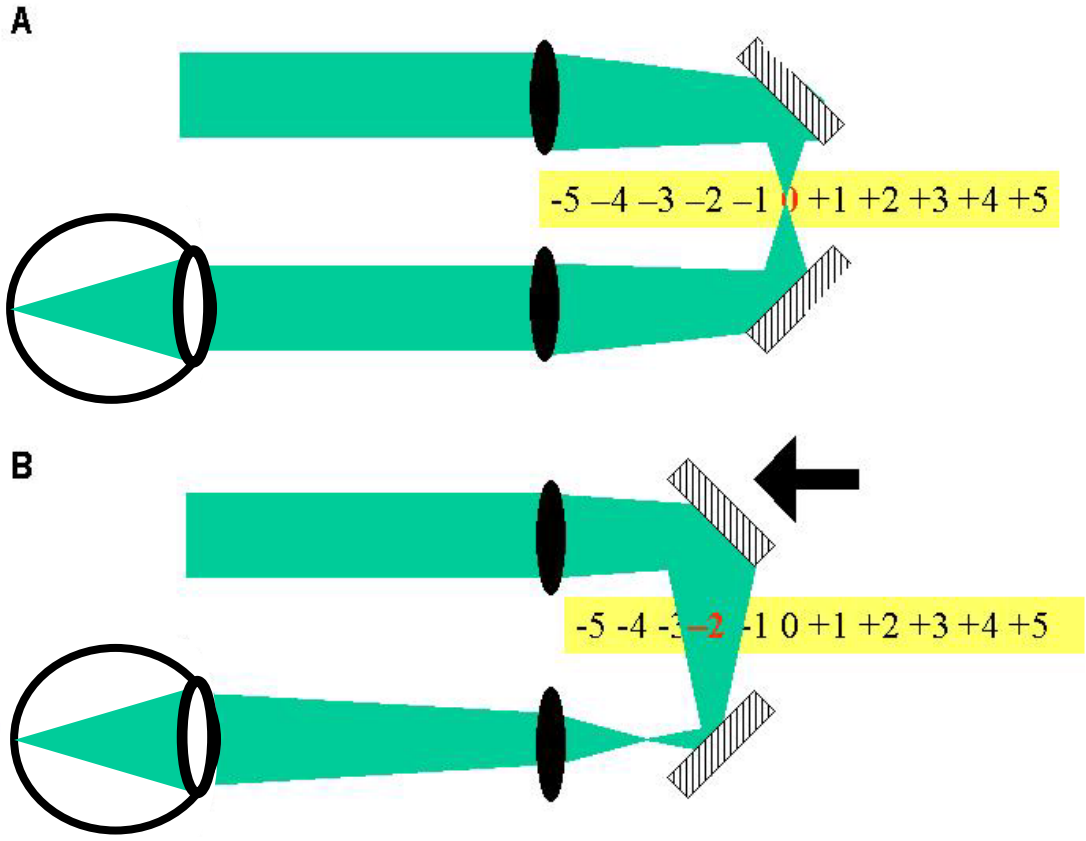

Figure 2.3 A- Badal position for an emmetropic eye. B-Badal position to correct a myopic eye.

vertical and horizontal axes lengths (Newport, 13E20-ER2 with reflectivity more than 98.5%) and two lenses (L1 & L2) (Newport, PAC055, 125 mm of focal length and a diameter of 25.4 mm). The mirrors were mounted on a rail and they were displaced to compensate for refractive errors. A displacement of 7.81 mm on the rail was equivalent to a focus shift of 1 D. The system could correct from -10 D to +10 D. Figure 2.3 shows an scheme of Badal position for emmetropic eye (A) and the position for correction of a myopic eye (B).

2.1.1.3. Pupil monitoring

The pupil monitoring channel was inserted in the system by means of two plate beam splitters (BS1 & BS2, Newport). The pupil was illuminated by 8 LEDs (Luminiscent Electric Diode) mounted on a 48-mm diameter ring (LR) placed in front of the eye and a camera (C2). The camera (Qcam, Logitech, Romanel-sur-Morges, Switzerland) has a color CMOS sensor of 1/5'' size, a resolution of 352 x 288 pixels and 43º of field of view. The USB interface permitted an easy and fast communication with the computer. The camera lens was replaced by a custom-built system with an objective built with two concentric aluminium cylinders and a lens (50.8mm focal length and diameter= 25.4mm lens diameter) (Newport, PAC040). Images of the pupil plane were magnified by a factor of x2. The camera allowed continuous viewing of the pupil and was used to center the eye immediately before the image capture.

2.1.2. Automatic control and data processing

Cameras, shutter and image capture were controlled by a program developed in Visual Basic. The Interface program permitted grabbing pupillary images, closing and opening the shutter and capturing the Hartmann-Shack retinal images. When the eye appeared aligned in the pupil monitoring camera, the software allowed rapid opening of the shutter, Hartmann-Shack image capture and saving and shutter closing. Figure 2.4 shows a typical screen capture of the control software.

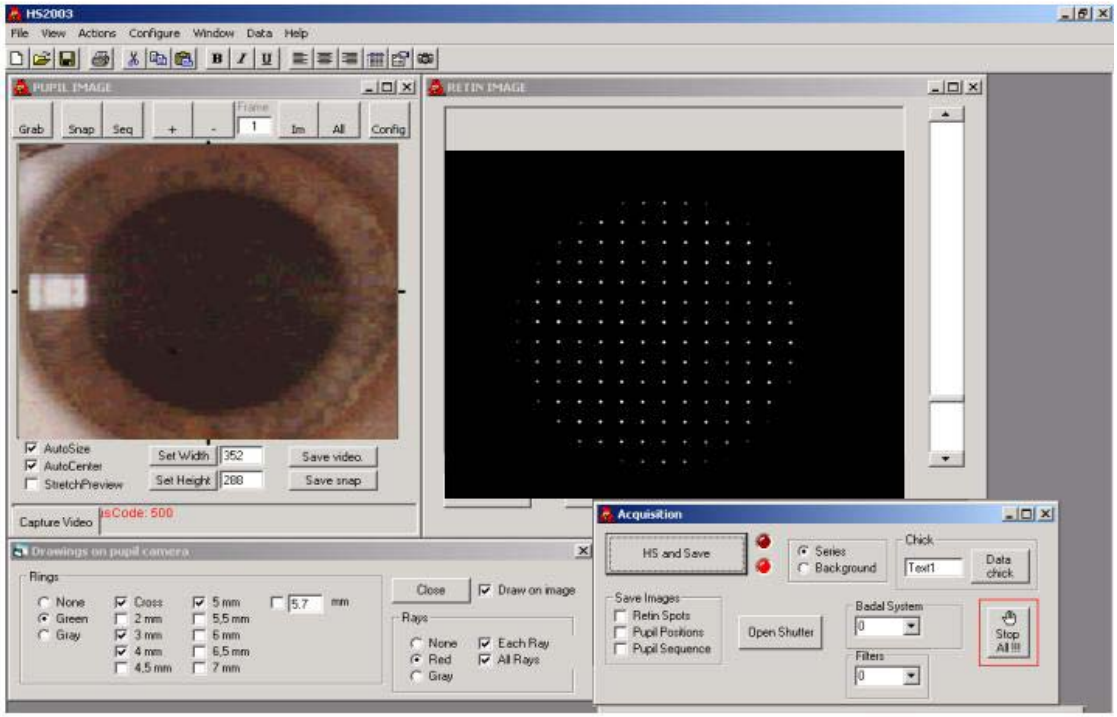

Figure 2.4 Screen capture from the control software.

The Hartmann-Shack spot images were processed using custom routines written in Matlab. The processing routines comprise the following steps, described graphically in Figure 2.5: 1) The retinal image was automatically divided in cells, each cell corresponding to the field of view of each microlens. For an ideal optical system (with no aberration) each HS spot should lie in the center of the cell. 2) Each spot image was detected automatically and fitted to a 2-dimensional gaussian function. The centroid was estimated as the peak location of the gaussian function. 3) The goodness of the fit to a gaussian function was estimated and a rejection criterion for eliminating spots corresponding to cells were the fitting parameter was below a threshold.

Typical situations in which the goodness of the fit was below threshold corresponded to situations in which there was light leakage from an adjacent cell, two spots in a cell, saturated images with non gaussian intensity profile, cells with no spots etc…4) From the centroids the aberration ray of each pupil position was estimated as the angular distance between the centroid of the

corresponding aerial image and the ideal location. The calibrated scale at the retinal image plane is 1 mrad = 0.024 mm. 5) The wave aberration was reconstructed from ray aberrations by a polynomial Zernike modal fitting.

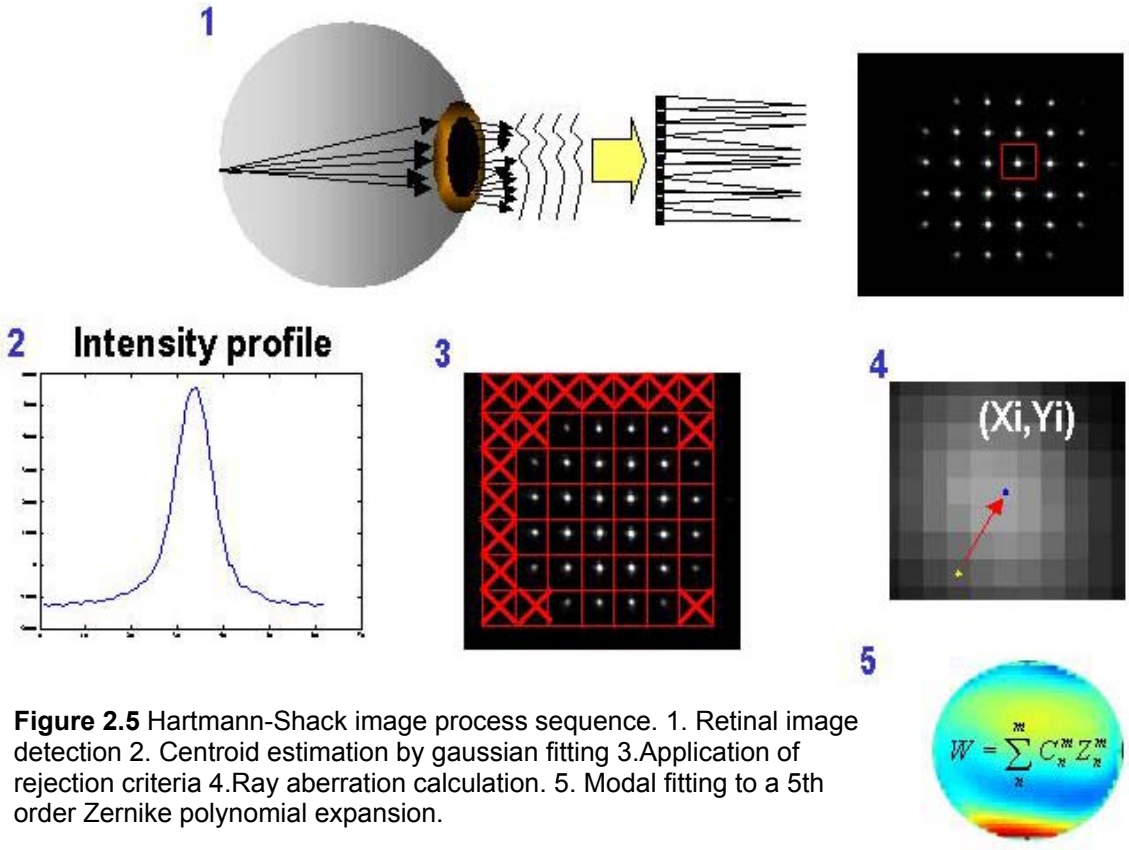

Figure 2.5 Hartmann-Shack image process sequence. 1. Retinal image detection 2. Centroid estimation by gaussian fitting 3.Application of rejection criteria 4.Ray aberration calculation. 5. Modal fitting to a 5th order Zernike polynomial expansion.

2.1.3. Alignment and calibration of the system

A systematic alignment was performed to ensure proper centration (at any position of the Badal system), and accurate location of pupil and retinal conjugate planes. Also, the system was calibrated using trial lenses, phase plates and artificial eyes with known aberrations.

2.1.3.1. Placing the micro array and CCD cameras

CCD camera C1 was placed on a x-y micrometer stage. First, the optical axis of the system was identified, and centered on the CCD chip. The location of the microlens array (a pupil conjugate plane) was found using a calibrated grid, the CCD camera and the focusing block, as the plane where

the magnification of the images of the grid captured by the CCD was constant

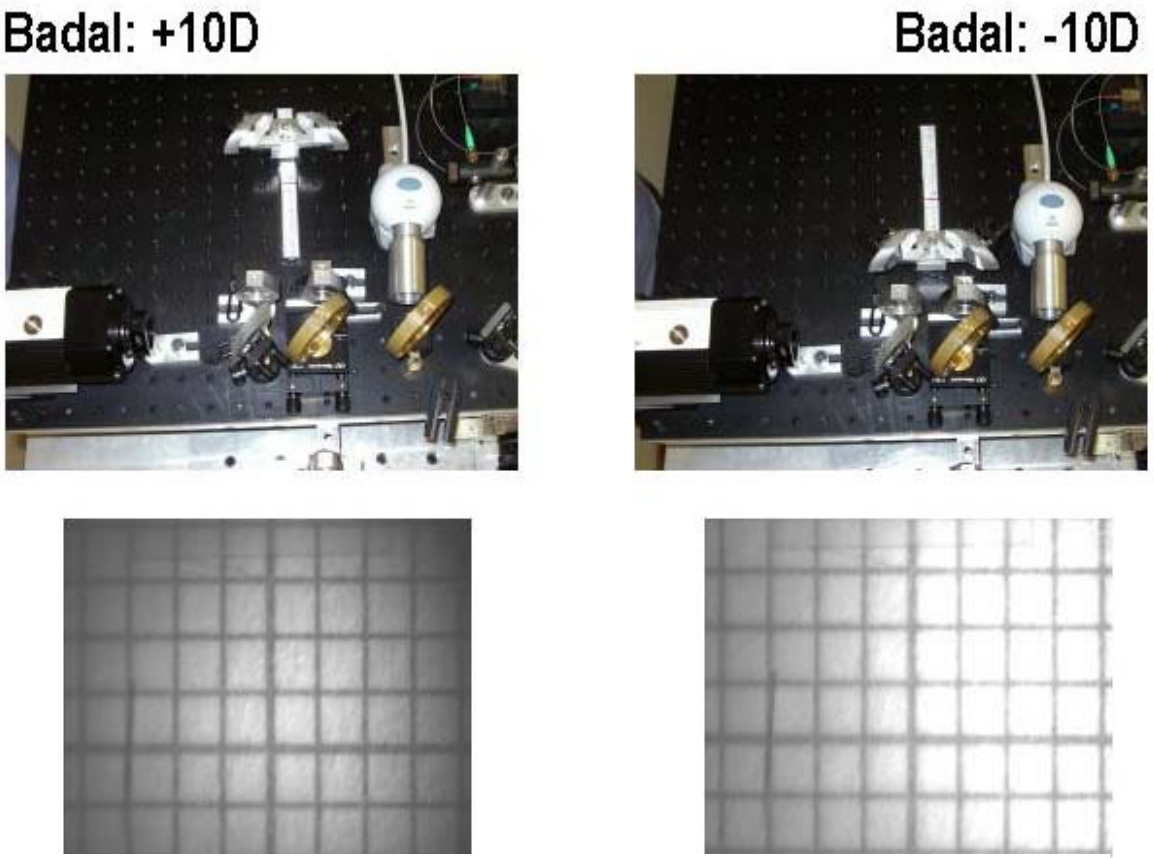

Figure 2.6 Images of the calibrated grid from two different positions of the Badal system during the set-up alignment.

regardless the position of the focusing block.

Figure 2.6 shows two images of the calibrated grid placed at the pupil plane, for two different positions of the focusing Block (0D and -10 D). Once this position was found, the pupil camera (C2) was placed in the pupil monitoring channel in such a way that both cameras captured the same test images and were collinear

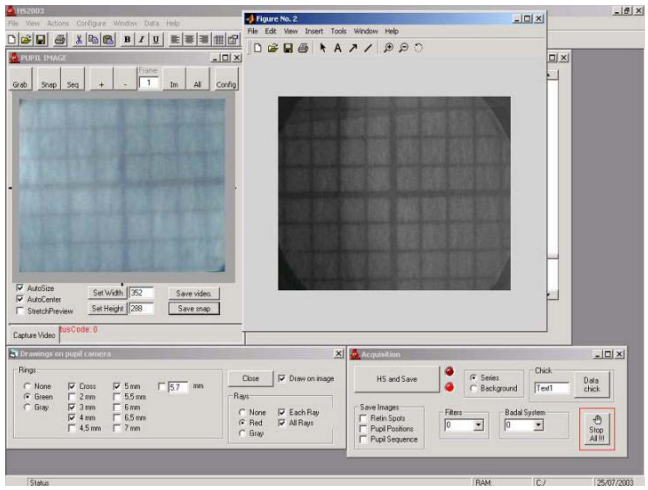

Figure 2.7 Images of simultaneous test grid by the retinal camera (C2, left) and the pupil camera (C1, right).

with the optical axis of the system (see Figure 2.7). Finally, we moved the CCD camera back 24 mm (i.e., the focal distance of the microlens array) along the optical axis, and placed the microlens array on the pupil conjugate plane. The alignment of the system was checked again, with an artificial eye (described in the next section), ensuring that the central spot of the retinal grid image (which is collinear with the optical axis of the camera) did not move across different positions of the Badal system.

2.1.3.2. Artificial eye

An artificial eye was built for validations and calibrations of the system. It consisted of an achromatic lens of 12.7 mm of diameter and 50.8 mm focal length (Newport, PAC028) and an aluminium cylinder. At the end of the cylinder a diffuser acted as a retinal back-reflector. A screw allowed to move the "retina" in the axial dimension. to simulate different refractive conditions. All Zernike terms measured for this eye were significantly different from zero. In particular, at best focus Z_{20} and Z_{40} were <0.01microns.

2.1.3.3. Calibration of the Badal System

We checked that the Badal system did not introduce magnification errors in the system and that the defocus corrections matched the theoretical predictions. The calibration of the Badal system involved the following steps: 1) We measured the separation between spots when the Badal lenses L1 and L2 were removed. The measured distance was 400 microns, the nominal separation between the centers of the microlenses. 2) With the lenses back in the system, we used the artificial eye described in section 2.1.3.2. to set up the zero position of the Badal system (where the spot separation is 400 microns). 3) We estimated the second order wave aberrations for the artificial eye and 10 different positions of the Badal optometer. We verified with equation 2.1 (Thibos et al. 2002):

$$M = \frac{-Z_{20}4\sqrt{3} + Z_{40}12\sqrt{5} - \ldots}{r^2} \qquad \text{Eq (2.1)}$$

that the mirror displacement was 7.81 mm/diopter, which matched the theoretical estimation

2.1.4. Validation of aberration measurements

We checked that the Hartmann-Shack system measured low and high order aberrations accurately. We used the artificial eye described in Section 2.1.3.2, provided with spherical and cylindrical trial lenses, as well as three Polymethyl methacrylate (PMMA) test eyes with known high order aberrations (Campbell 2005).

2.1.4.1. Sphere and cylinder measurements

Data were obtained for the artificial eye described in section 2.1.3.2 with spherical trial lenses placed in a pupil conjugate plane. Defocus was obtained from Zernike coefficients using equation (2.1). Figure 2.8 (A) shows defocus for the different trial lenses under test ranging from –3.25 D to +4 D. Additional measurements were performed using cylindrical lenses with the non-aberrated artificial eye, which were used to check that the measured amount of astigmatism and axis were correct (examples for +2 and +3D cylindrical lenses are shown in Figure 2.8 (B)). Average differences between measured cylinder and nominal values were: -0.21 ± 0.22D, and average difference in the axis was 3.5 ± 3.1 degrees.

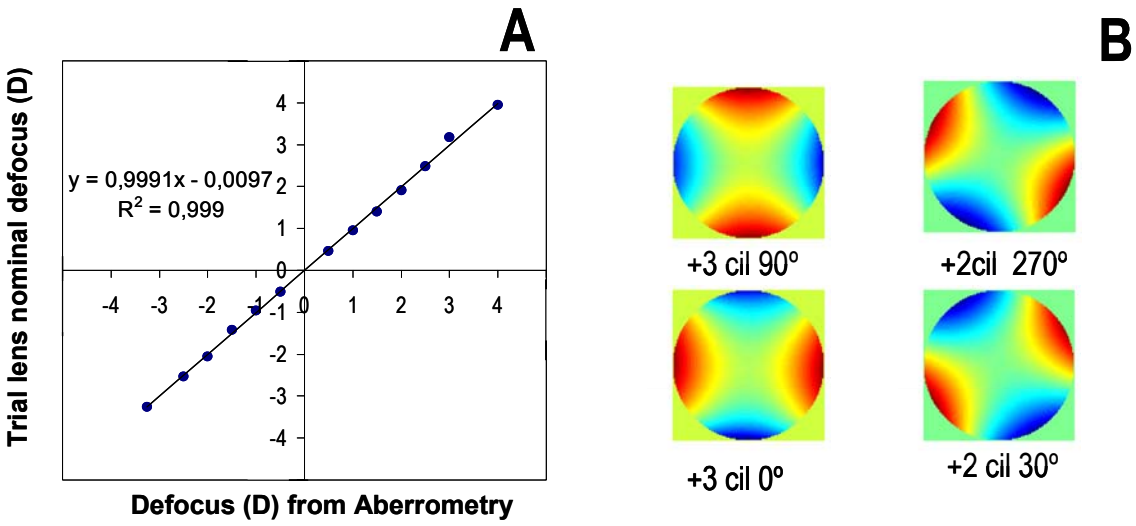

Figure 2.8 A. Trial lens defocus vs. defocus obtained by Zernike coefficients. B. Aberration maps for several cylindrical trial lenses.

2.1.4.2. High order aberrations

The accuracy of our Hartmann Shack system in measuring high order aberrations was studied using PMMA artificial eyes with known aberrations provided by Charles Campbell (Berkeley, CA, USA). These test eyes were designed as rods with a convex front surface with a radius of curvature similar to the human cornea (7.8 mm) and 12.7 mm of diameter (Campbell 2005). The back surface ("retinal plane") is polished and painted with black paint. Three eyes were tested: A4 with a simple spherical front surface, and nominally only with coefficients Z_{20} and Z_{40} significantly different from zero; A3 (cast) and L2 (extruded) lathed with significant amounts of high order aberrations in terms Z_{20}, Z_{40}, Z_{51} and Z_{62}. The eyes had been calibrated using numerical ray tracing on the surface elevation maps, and measured by different commercial aberrometry techniques in a published multi-site study by Campbell (Campbell 2005). The reference values were obtained by averaging results from the different instruments. Figure 2.9 shows a comparison of Zernike coefficients from the average reported values and those obtained with or our Hartmann Shack system.

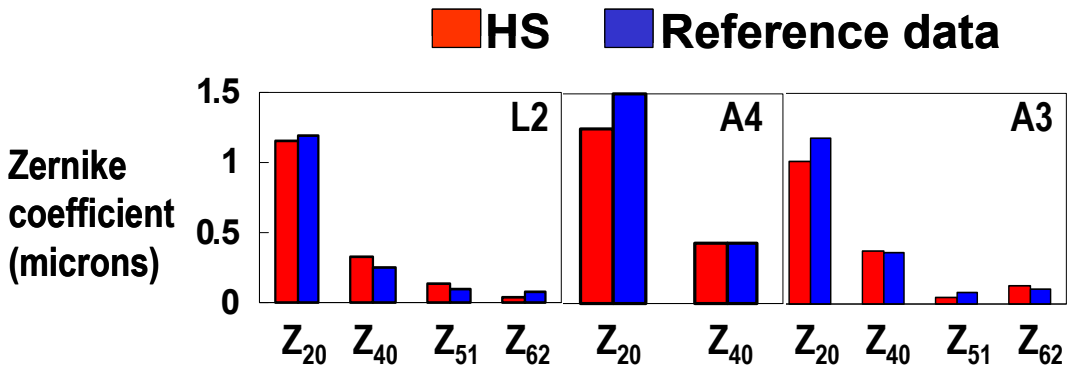

Figure 2.9 Comparison of high order aberrations form our Hartmann-Shack aberrometer and nominal data for a PMMA artificial eye (provided by C.Campbell)

2.2. Measurement of biometric parameters

In addition to ocular aberrations, the measurement of other biometric parameters was essential to assess the ocular dimensions and power during natural development or following treatment in experimental animal models (under awake conditions). We implemented techniques to measure axial length and corneal radius of curvature, as well as refractive error in animal models.

2.2.1. Refractive error

In this thesis we present measurements of refractive error from two different techniques: retinoscopy and based on aberrometry when retinoscopy was not possible (in chick refractive surgery and mouse models).

2.2.1.1. Streak Retinoscopy

Retinoscopy is an objective technique to evaluate spherical and cylindrical refractive error. It consists of neutralizing the movement of pupil reflex with trial lenses while sweeping the scope across the pupil. If the streak appears to be moving against the direction of the scope, minus lenses are required, and the opposite when the reflection moves with the scope. If there is no apparent motion, neutrality has been reached. The procedure can be repeated on any meridian to obtain astigmatism. This clinical technique had been widely used in chicks before (Yinon et al. 1980).

Figure 2.10 The author performing a chick retinoscopy measurement

In this thesis we performed retinoscopy measurements under natural viewing conditions (no anaesthesia, no cycloplegia, nor

lid-retractors). Figure 2.10 shows a chick retinoscopy measurement in the laboratory.

2.2.1.2. Spherical equivalent from aberrometry

Refraction was obtained in some experiments as the spherical equivalent from a wave aberration measurement, added to the defocus compensated by the Badal system (see section 2.1.1.2). The spherical equivalent of the wave aberration is defined as the quadratic surface which best represents the wave aberration map, obtained by minimizing the sum of squared deviations between the wave aberration and the quadratic surface. The least square solution is given by the second order Zernike coefficients and can be converted to sphere using equation 2.1, and cylinder at 0º and 45º with equations 2.2 and 2.3, respectively (Thibos et al. 2002).

$$J_0 = \frac{-Z_{22}2\sqrt{6} + Z_{42}6\sqrt{10} - \ldots}{r^2} \quad \text{Eq. (2.2)}$$

$$J_{45} = \frac{-Z_{2-2}2\sqrt{6} + Z_{4-2}6\sqrt{10} - \ldots}{r^2} \quad \text{Eq. (2.3)}$$

2.2.2. Axial length: Biometry

To evaluate eye length is important to assess ocular growth due to natural development in control eyes and treatment-induced elongation in treated eyes. We measured axial length in awake chicks with a standard ultrasound biometry (for measurements in humans) adapted to chick eye's dimension, using a technique

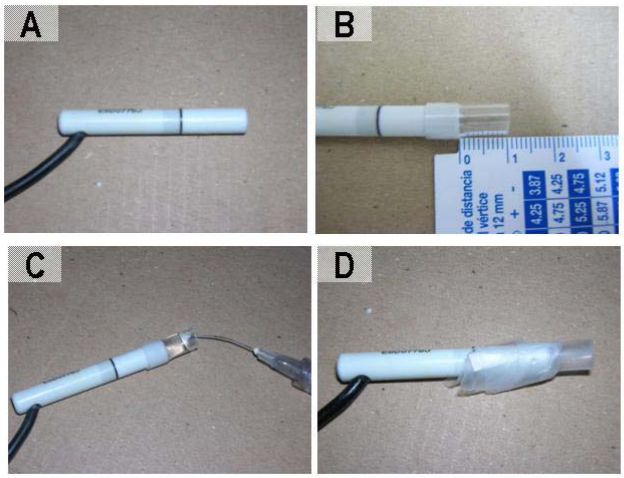

Figure 2.11 Biometer probe adapted. A. Normal probe. B. Plastic tube extension. C. Filling the tube with water. D. Covered with paraffin film.

proposed by Schaeffel et al (Schaeffel and Howland 1991). We used an Allergan Humphrey ultrasound biometer (Mod. 826) with a custom-adapted probe. A 10-mm plastic tube was attached to the probe, filled it with water and covered with paraffin film, as described in the literature (Schaeffel and Howland 1991), and illustrated in Figure 2.11. This technique requires topical anaesthesia due to the contact between the probe and the cornea. Figure 2.12 shows the author of this thesis performing an ultrasound biometry measurement on a chick and a typical result on the display of the commercial instrument. In normal clinical measurements two peaks are obtained, indicating two interfaces: probe-cornea and vitreous-retina. The distance between these peaks is the axial length. In the instrument with the adapted probe and additional peak is obtained, resulting from the tube extension - original probe interface. We subracted the tube extension length from axial length indicated by the biometer to obtain axial length in small animal eyes. For each measurement the isolated tube length was measured, by capturing a tube measurement with the tube immersed in a water recipient.

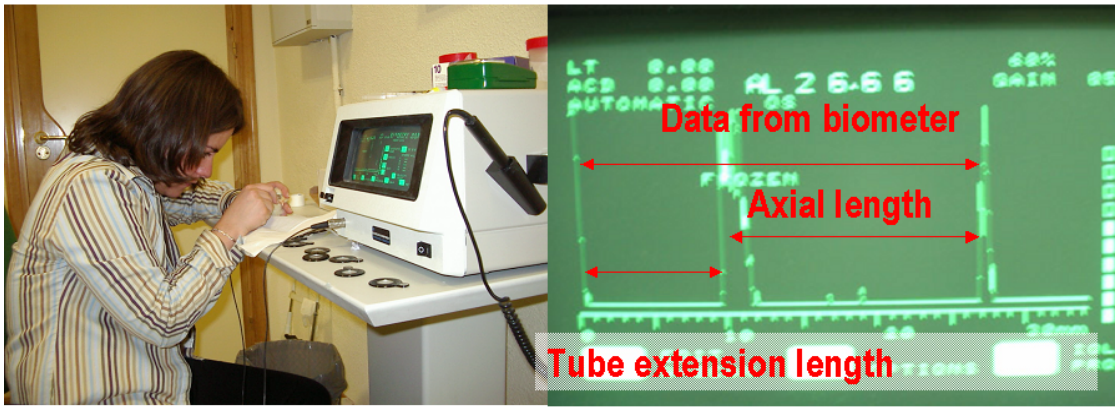

Figure 2.12 Picture of a biometric measurement on a chick and an image of the ultrasound screen.

2.2.3. Corneal radius: Keratometry

For this thesis we also implemented a custom-built infrared (IR) photokeratometer to measure corneal curvature in the chick eye. This method has been applied in animal models previously, and it is described by Schaeffel and Howland (Schaeffel et al. 1986; Schaeffel and Howland 1987). Our keratometer consists of a ring of eight Infrared (IR) LEDs placed around a

circumference of 80 mm diameter and an 8-bit CCD camera (Toshiba Teli America, 1360 x 1023 pixels, Irving, California, USA) provided with a 105 mm focal length camera lens (Rodenstock) and extension tubes (70 mm). A schematic dia gram of the system is depicted in Figure 2.13. The image capture was controlled by the computer using a program written in Visual

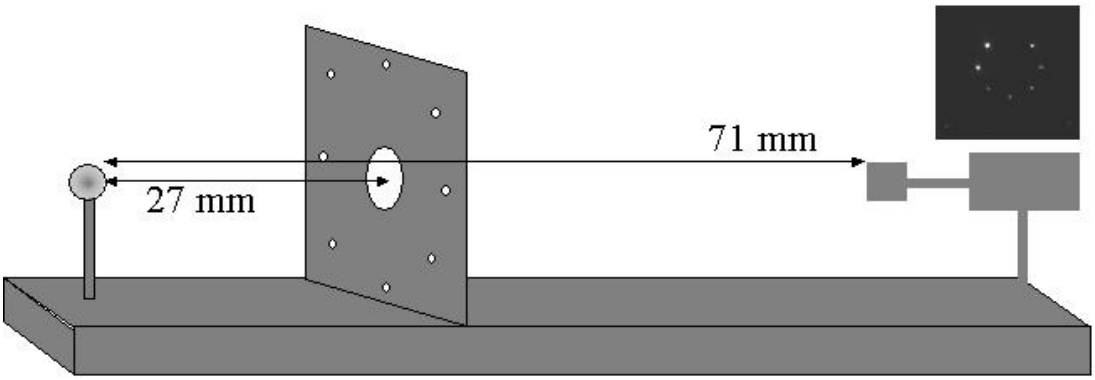

Figure 2.13 A schematic diagram of the implemented keratometer

Basic (Microsoft Corporation, Redmond, Washington). Figure 2.14 shows a screen capture of the software. The pupillary images were processed using routines written in Matlab (Mathworks, Nattick MA). The Purkinje images of the LEDs were detected, and their positions were automatically estimated using a centroiding algorithm. The system was calibrated using a set of calibrated steel spheres, and the calibrated curves were used to convert from the ring diameter on the image (average radial distance between LED image locations) to corneal radius of curvature. Figure 2.15 (A) shows a typical image from a steel sphere and (B) the calibration curve which relates radius of the LEDs circle image with the nominal sphere radius. The diameter of the LED ring on the image was computed, using a scale of 0.019 mm/pixel. The conversion factor, obtained from a linear regression to the data of Figure 2.15 (B) was: 1 mm (ring diameter) / 3.9 mm (corneal radius of curvature).

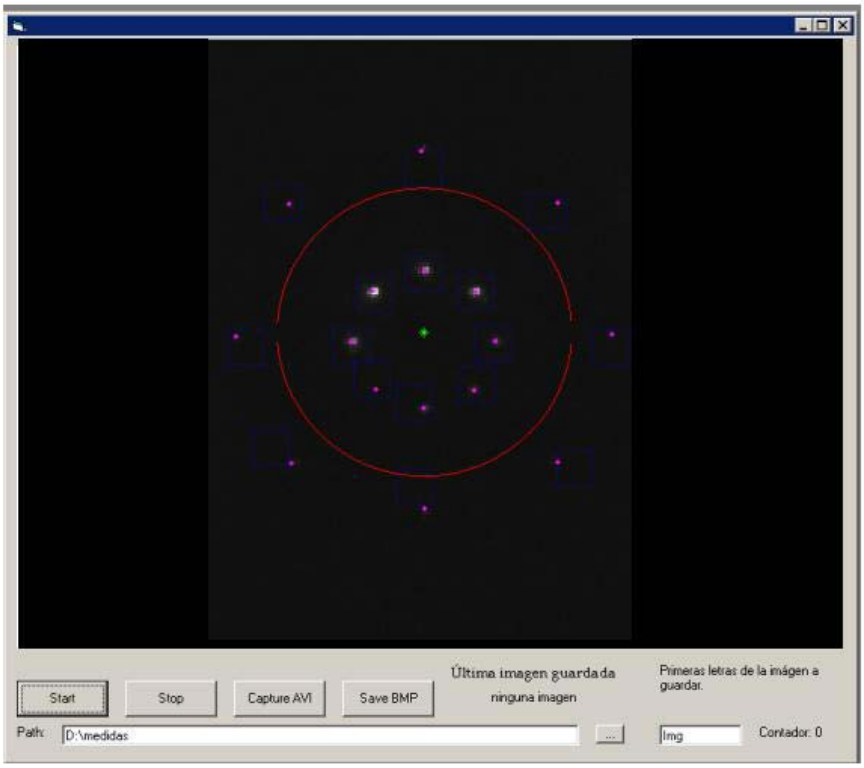

Figure 2.14 An example of a keratometric image from as captured by the custom keratometer software.

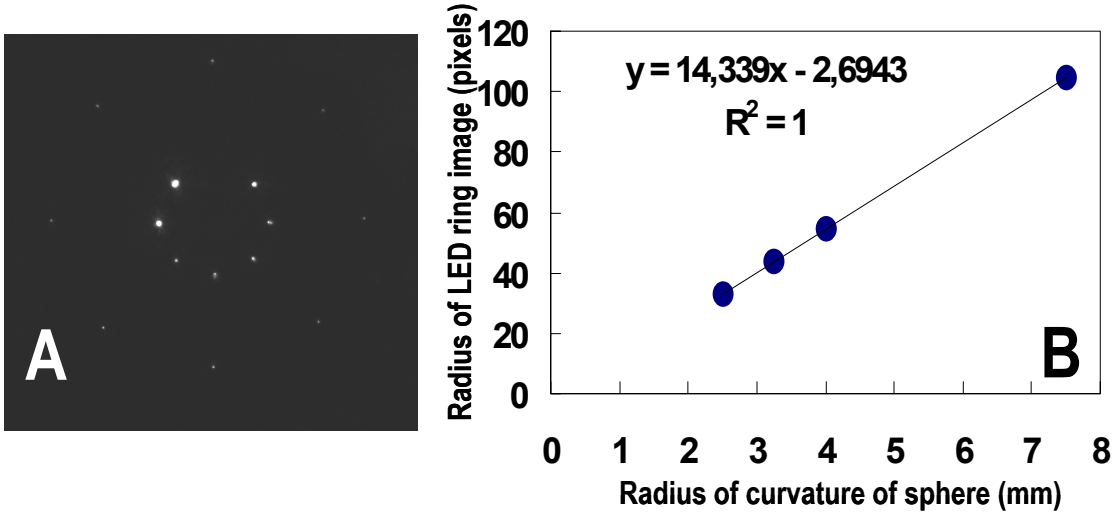

Figure 2.15 A. image from a calibrated steel sphere. B.Calibration curve (radius of the LEDs circle image vs. nominal sphere radius).